JOURNAL OF GEOPHYSICAL RESEARCH, VOL. 113, A09223, doi:10.1029/2008JA013038, 2008

Erosion of the dayside magnetosphere at Mercury in association with ion outflows and flux rope generation

A. Kidder,[1] R. M. Winglee,[1] and E. M. Harnett[1]

Received 15 January 2008; revised 10 June 2008; accepted 11 July 2008; published 23 September 2008.

[1] In preparation for the arrival of the MESSENGER spacecraft at Mercury, and to further understanding of the Mariner 10 and ground-based observations, 3-D multifluid simulations are used to predict Mercury's magnetospheric response to forcing from the solar wind. The model, which includes both heavy (Na^+) and light (He^+) ionospheric ion populations, predicts that solar wind access to Mercury's surface is highly asymmetric and dependent on the strength and direction of the interplanetary magnetic field (IMF). In particular, during southward IMF much of the dayside magnetic field can be eroded, and enhanced plumes of sodium ions (with geometry similar to ground-based emission observations) outflow at high latitudes into the solar wind. Development of reconnection in association with flux ropes similar to those at Earth are seen but with a shorter time scale of development and a closer radial distance ($3-5$ R_M).

Citation: Kidder, A., R. M. Winglee, and E. M. Harnett (2008), Erosion of the dayside magnetosphere at Mercury in association with ion outflows and flux rope generation, *J. Geophys. Res.*, *113*, A09223, doi:10.1029/2008JA013038.

1. Introduction

[2] Observations from the Mariner 10 spacecraft in the mid-1970s [*Ness et al.*, 1975] and the McMath-Pierce Solar Telescope in the 1980s [*Potter and Morgan*, 1985, 1986] provide detailed data on the interaction of Mercury's magnetosphere with the solar wind. Numerical simulations of the Hermean system build upon this observational knowledge in preparation for the upcoming MESSENGER and Bepi-Colombo missions to the planet. Mercury has a tenuous ionosphere including He^+, Na^+, O^+, K^+, and Ca^+ components [*Lundin et al.*, 1997]. Its intrinsic global magnetic field is of equatorial surface strength $\sim$330 nT; while this is two orders of magnitude less than the terrestrial field, appears strong enough to stand off the solar wind under typical conditions ($n \approx 30$ cm^{-3}, $v \approx 430$ km/s, $B_{IMF} \approx 20$ nT). The consequence of a weak magnetic field, with the high density and dynamic pressure of the solar wind at Mercury's orbital radius, is that the Hermean magnetospheric cavity is significantly smaller than Earth's magnetic cavity, relative to the size of the planet. It is suspected that southward IMF erodes the dayside magnetosphere, causing the solar wind stand-off distance to move inward by $\sim$2000 km [*Slavin and Holzer*, 1979]. MHD and hybrid simulations have previously needed extreme solar wind conditions (velocities of 860 km/s and 1100 km/s, respectively) to obtain direct impact of solar wind protons [*Kallio and Janhunen*, 2003b; *Kabin et al.*, 2000].

[3] Ground-based measurements of Mercury's exosphere show a sodium population density of $\sim 10^4$ cm^{-3} [*Hunten et al.*, 1988] with a spatial distribution that changes over several nights [*Potter et al.*, 1999]. Proposed explanations of this phenomenon include impact vaporization, photon-stimulated desorption, and sputtering of sodium ions from the surface by incoming solar wind protons [*Killen and Ip*, 1999]. The UV spectrometer aboard Mariner 10 observed hydrogen, helium and oxygen in Mercury's near space environment [*Broadfoot et al.*, 1974]. *Potter et al.* [1999] observed the evolution of neutral Na plumes over several days. Our model shows that Na^+, created from neutral Na close to the surface, moves along magnetic field lines into plumes at the poles. It is this Na^+ which is subsequently converted back to Na through charge exchange that can produce the Na plumes observed from Earth.

[4] The Mariner 10 mission demonstrated startlingly rapid time scales over which Mercury's magnetosphere evolves. The first flyby traversed the magnetotail in a seventeen minute dusk-to-dawn pass, during which the IMF switched from northward to southward and substorm signatures were seen in both the magnetometer and plasma data [*Russell et al.*, 1988]. During such a flip in the orientation of the IMF, *Russell et al.* [1988] calculated that the bow shock will move inward from 1.9 R_M to 1.3 R_M, measured from the center of the planet (1 R_M = 2440 km). Alternately, *Luhmann et al.* [1998] assert that these signatures arose from a "driven" process, unlike "triggered" terrestrial substorms. While waiting for MESSENGER [*Solomon et al.*, 2001] to bring definitive evidence either way, we examine magnetospheric dynamics on minute time scales.

[5] This paper uses multifluid simulations of northward and southward IMF to examine erosion of magnetic flux in the dayside magnetosphere by the solar wind, and the effect of IMF orientation on ion outflow and flux rope generation. The multifluid treatment includes ion cyclotron and heavy ion effects, making it the ideal tool for examining the

[1]Department of Earth and Space Sciences, University of Washington, Seattle, Washington, USA.

0148-0227/08/2008JA013038$09.00

Hermean system which combines a weak magnetic field with a population of heavy ions. These effects are shown to produce significant asymmetries in solar wind proton precipitation that varies with IMF configuration. The model shows substantial IMF direction dependent magnetospheric variation. Flux ropes with a core magnetic field are generated within minutes of the IMF turning southward. The location of the reconnection line is several Hermean radii downstream, and outflow of sodium ions at high latitudes are seen that may be indicative of a connection between the magnetosphere and the variable Na^+ population.

2. Model

[6] To examine the effect of the solar wind and IMF conditions on the morphology of the planetary field and heavy ion outflow it is necessary to include plasma dynamics on a global scale while still incorporating the dynamics of multiple ion species (which exhibit themselves on small scales). The multifluid model employed here for the Hermean system was described by *Winglee* [2004] for terrestrial applications. It has more recently been used to study weakly magnetized systems, e.g., Pluto [*Harnett et al.*, 2005], Ganymede [*Paty and Winglee*, 2006], and Mars [*Harnett and Winglee*, 2007].

[7] The simulation simultaneously tracks three separate ion fluids and an electron fluid. In Mercury's system these ion species are the solar wind protons (H^+), a light ion population from Mercury assumed to be helium (He^+), and a heavy ion population from Mercury assumed to be sodium (Na^+). The inclusion of mass effects, using a modified Ohm's law and ion cyclotron effects in the full conservation of momentum equation, allows us to track the manner in which different ions are accelerated.

2.1. Multifluid Treatment

[8] Multifluid equations (1)–(3) track the individual components of the plasma through separate conservation equations for mass, momentum and pressure. The subscript α denotes the various ion species that constitute the plasma.

$$\frac{\partial \rho_\alpha}{\partial t} + \nabla \cdot (\rho_\alpha \vec{v}_\alpha) = 0 \tag{1}$$

$$\rho_\alpha \frac{d\vec{v}_\alpha}{dt} = n_\alpha q_\alpha \left(\vec{E} + \vec{v}_\alpha \times \vec{B}\right) - \nabla P_\alpha - \left(\frac{GM_M}{R^2}\right)\rho_\alpha \vec{r} \tag{2}$$

$$\frac{\partial P_a}{\partial t} = -\gamma \nabla \cdot (P_a \vec{v}_a) + (\gamma - 1)\vec{v}_\alpha \cdot \nabla P_a \tag{3}$$

where ρ_α is the mass density, v_α the bulk velocity, n_α the number density, and q_α the charge. G is the gravitational constant, M_M the mass of Mercury, R the planetary radius, $\vec{E}$ the electric field, $\vec{B}$ the magnetic field. P_α is the pressure for each ion species and γ is the ratio of specific heats (5/3).

[9] The electron dynamics are determined by a pressure equation where the electrons have sufficiently high mobility along the field lines such that they are approximately in steady state (i.e., $dv_{de}/dt = 0$), or in drift motion:

$$\frac{\partial P_e}{\partial t} = -\gamma \nabla \cdot (P_e \vec{v}_{de}) + (\gamma - 1)\vec{v}_{de} \cdot \nabla P_e \tag{4}$$

where P_e is the electron pressure and v_{de} the electron drift speed.

[10] Approaching this limit the modified Ohm's law becomes:

$$\vec{E} = -\sum_i \frac{n_i}{n_e}\vec{v}_i \times \vec{B} + \frac{\vec{J} \times \vec{B}}{en_e} - \frac{\nabla P_e}{en_e} + \eta(\vec{r})\vec{J} \tag{5}$$

where n_e is the electron number density, e the electron charge, $\vec{J}$ the current density, and η is the resistivity, added to allow finite conductivity only in the ionosphere. The resistivity is zero at all other locations, thus there is no anomalous resistivity in our model. The Hall and pressure gradient terms in Ohm's Law (5) are sufficient to drive reconnection. On substituting (5) into the momentum equation we obtain:

$$\rho_\alpha \frac{d\vec{v}_\alpha}{dt} = \frac{q_\alpha n_\alpha}{en_e}\left(\vec{J} \times \vec{B} - \nabla P_e\right) - \nabla P_\alpha + q_\alpha n_\alpha \left(\vec{v}_\alpha - \sum_i \frac{n_i}{n_e}\vec{v}_i\right) \times \vec{B} + q_\alpha n_\alpha \eta \vec{J} - \left(\frac{GM_M}{R^2}\right)\rho_\alpha \vec{r} \tag{6}$$

If one assumes a single ion species, (6) reduces to the ideal MHD equations. The different ion species may take different ion velocities and the middle term, assumed to be zero in MHD, is in fact nonzero and contributes to the dynamics identified between the different ion species below.

2.2. Boundary and Initial Conditions

[11] The equations for this multifluid treatment are solved with a second-order Runge-Kutta method, on a "nested grid" in Cartesian coordinates where Mercury is situated within the region of highest resolution. The inner boundary is set to 1 R_M (the planet's surface). With the origin at the center of the planet, the positive x-direction points with the solar wind flow, the positive y-direction points in the dawn-direction and the positive z-direction points northward. This grid system has the highest resolution (~120 km) over the inner magnetosphere (from -2.2 R_M sunward to 2.2 R_M downtail, ±2.2 R_M in the dawn-dusk y-direction and ±1.9 RM over the poles), while permitting the global view to extend from -9 R_M sunward to 35 R_M downtail, ±17.6 R_M in the dawn-dusk y-direction, and ±15.2 R_M over the poles. The conductivity [*Krall and Trivelpiece*, 1973], was set to be 4×10^{-4} mhos/m at the ionosphere, and zero everywhere else in the simulation.

[12] For initial conditions we assume that Mercury's tenuous ionosphere has densities at the planet's surface of 13 cm^{-3} (light ions) and 50 cm^{-3} (heavy ions) with a Maxwellian distribution, on the basis of the ion estimates given by *Lundin et al.* [1997]. The temperature gradient ranges from 20 eV at the equator to 1 eV at the poles, and the electron temperatures are half of these values. The temperature is held constant at the inner boundary, but since each species is its own fluid, they evolve with different temperatures and velocities above the inner boundary. The

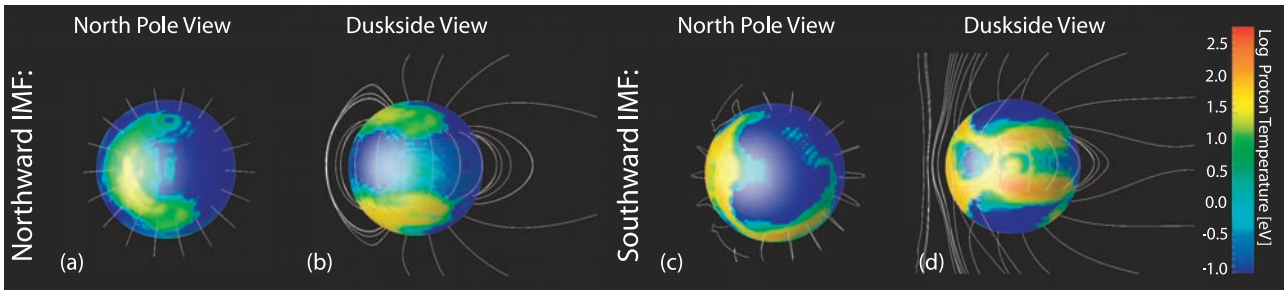

Figure 1. Movement of solar wind proton precipitation from higher to lower latitudes under northward (Figures 1a and 1b) and southward (Figures 1c and 1d) IMF. Color bar indicates H^+ temperature at 1 R_M. White magnetic field lines show erosion of magnetic flux on the dayside with a view of the (a) equatorial plane and (b) noon-midnight meridian for northward IMF and of the (c) equatorial plane and (d) noon-midnight meridian for southward IMF.

two populations are coupled in the Ohm's law (equation (5)). The solar wind is injected from the sunward side of our model with a density of 40 cm^{-3} at a constant speed of 450 km/s with a temperature of 17 eV. The inner boundary assumes a plasma with prescribed density and temperature but no bulk velocity, which leads to a small thermal, or polar, wind. Enhanced outflow is produced if ion streams are heated or accelerated by magnetospheric processes. The planet is assumed to have a 330 nT dipolar magnetic field with the same polarity as Earth.

3. Results

3.1. Solar Wind Erosion of the Dayside Magnetosphere

[13] Figure 1 demonstrates the change in the morphology of the magnetic field between northward ($[B_x, B_y, B_z]$ = [0, 0, 15] nT) and southward ($[B_x, B_y, B_z]$ = [0, 5, −20] nT) IMF, where solar wind proton precipitation is visualized by mapping the proton temperature onto the planet's surface. For northward IMF the subsolar point of the bow shock and the magnetopause form at 1.8 R_M and 1.4 R_M, respectively. This agrees with *Russell et al.*'s [1988] calculated values of 1.9 R_M and 1.4 R_M. For southward IMF these values were found to be 1.3 R_M and 1.1 R_M, respectively. MHD models such as those of *Kabin et al.* [2000] and *Ip and Kopp* [2002] calculate bow shock positions farther out from the planet; at distances of 4.0 R_M and 2.2 R_M (for Parker spiral and northward IMF conditions). The multifluid model is able to more closely match observed bow shock positions as it includes ion-cyclotron effects such as pick-up of planetary heavy ions, which enhance ion loss and mass loading of the solar wind. A consequence of having bow shock and magnetopause positions so close to the planet is that for northward IMF, the closed field line boundary is at a latitude of ∼75°. During southward IMF, this boundary moves to a lower latitude of ∼65° and the open field lines at higher latitudes allow solar wind protons to precipitate at the cusps. This is lower than the cusp location at Earth, which can move down from 85° to 70° during active times, and is due to Mercury's weaker global magnetic field.

[14] Solar wind, in addition to the inward movement of the bow shock and magnetopause, erodes the dayside magnetosphere, transferring magnetic flux from the dayside to the magnetotail. During northward IMF, two distinct bands of increased temperature seen on the dayside indicate proton precipitation (Figure 1a). When the IMF is southward, the dayside sees the solar wind impact latitude decrease as the polar cap enlarges. The increased proton temperature region now covers much of the dayside. The nightside, however, sees very little temperature increase during northward IMF, as the high-latitude bands do not fully encircle the polar cap. When the IMF turns southward the polar cap enlarges and temperature increases at the equatorial region of the nightside. The hybrid model of *Kallio and Janhunen* [2003b], which included solar wind particles as the sole species, shows solar wind flux in bands similar to those in Figures 1a and 1b. Our model is in agreement that solar wind precipitation is low near the poles on the nightside and highest on the dayside. During southward IMF, the bands move to latitudes ∼60°, slightly equatorward of the open/closed field lines, most likely because both hybrid and multifluid models include ion cyclotron effects. The velocity of the solar wind at Mercury is similar at Earth, although the proton density and strength of the IMF are increased, which causes Mercury's polar cap to open to much lower latitudes than at Earth. Although Mercury lacks an atmosphere dense enough to support visible aurora, the Mercury Atmospheric and Surface Composition Spectrometer instrument on board the MESSENGER spacecraft will be able to confirm any UV emission in these areas [*McClintock and Lankton*, 2007].

3.2. Na^+ Outflow

[15] *Potter and Morgan*'s [1990] and *Potter et al.*'s [1999] ground-based observations saw the emission brightness of neutral exospheric sodium at low altitudes around Mercury change over the span of several days. The distribution of sodium emission grew asymmetrically, with two intense outflows originating at the cusp regions in the north and south hemispheres. It has been proposed that these high-latitude enhancements are controlled by magnetospheric processes which are regulated by the IMF [*Potter and Morgan*, 1990].

[16] The multifluid model quantifies the effect of the impinging solar wind and directional IMF on the dynamic behavior of the heavy sodium ion population. Mercury's tenuous ionosphere also contains He^+, presumably from the solar wind. In the model, this exospheric He^+ is seen to remain at low altitudes around originating the planet while the IMF is oriented in either direction. However, for the heavier Na^+ population the model predicts large plumes of

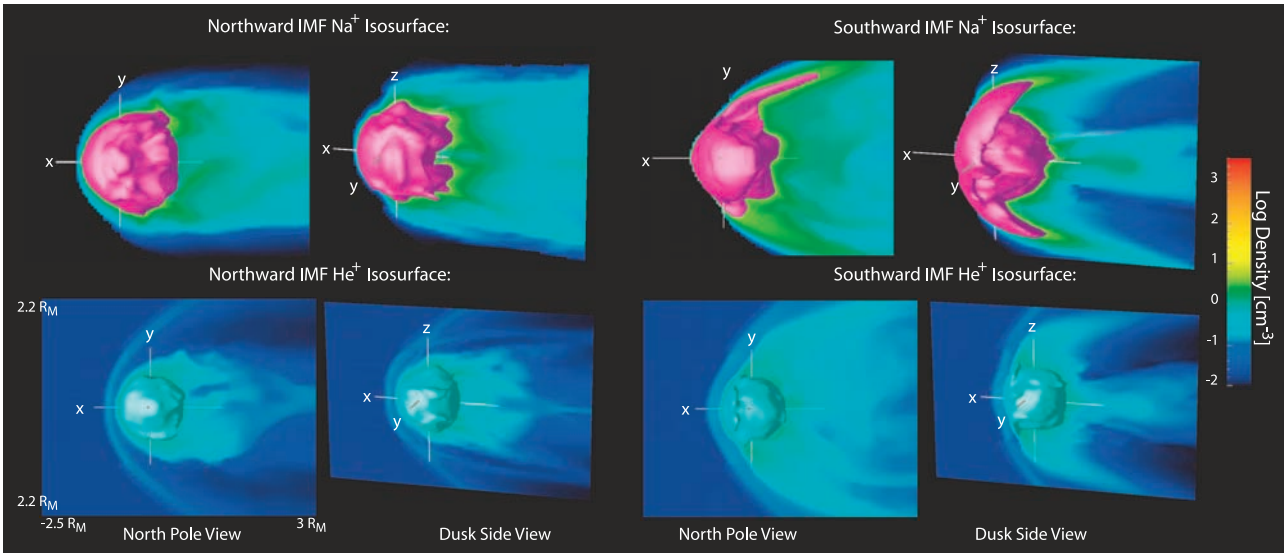

Figure 2. Development of ion outflow in the form of plumes in the heavy ion population (outflow seen during southward IMF for Na^+, but not He^+). Magenta (a surface with a constant density of 5 cm^{-3}) overlaid on Na^+ density plot is contrasted with cyan (a surface with constant density of 5 cm^{-3}) overlaid on a He^+ density plot for northward IMF (first column, equatorial plane; second column, noon-midnight meridian) and southward IMF (third column, equatorial plane; fourth column, noon-midnight meridian (note the high-latitude plumes in Na^+)).

Na^+ outflowing from high northern and southern latitudes during southward IMF. Figure 2 plots surfaces of constant density (5 ions/cm^3) of Na^+ (top row) and He^+ (bottom row) for views of the equatorial plane (first column) and the noon-midnight meridian (second column).

[17] By retaining the ion cyclotron effects in the electric field of our multifluid model, we are able to see asymmetries in both the densities and plasma convections of the different ion species. The initial conditions in this model assume a population of azimuthally symmetric tenuous sodium ions. The sodium ions move out into the magnetosphere and slowly downtail, but antiparallel (southward) magnetic field at the magnetopause is required to produce these enhanced heavy ion outflows.

[18] Figure 2 demonstrates that the heavier sodium ion population of the multifluid model remains relatively close to the planet during quiet times yet, during more active times, these sodium ions are picked up and greater densities are found in both the north and south hemispheres. Additionally, pick-up ions create a dawn-dusk asymmetry in the xy-plane because of the convection electric field (Figure 2d). The flux of the Na^+ plumes at high northern and southern latitudes is calculated to be $\sim 10^{23}$ ions/s for northward and $\sim 10^{24}$ ions/s for southward IMF.

[19] The sodium ion outflow in the model is consistent in geometry and variability with the neutral sodium emission seen in ground-based observations [*Potter et al.*, 2002; *Killen and Ip*, 1999]. The morphology of the neutral sodium and ion outflow may be compared (Figure 3) because heavy

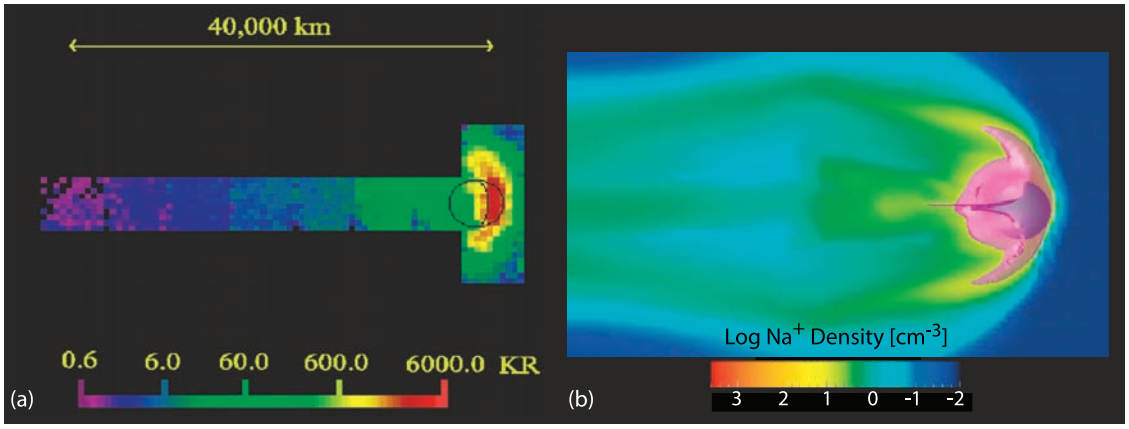

Figure 3. Comparison of the geometry for (a) Na emission brightness as observed from the McMath-Pierce Solar Telescope [from *Potter et al.*, 2002] (reprinted with permission from the Meteoritical Society) and (b) plot of Na^+ density in the noon-midnight meridian with a magenta surface of constant density (7 cm^{-3}) that highlights the ion outflow occurring in both the northern and southern hemispheres.

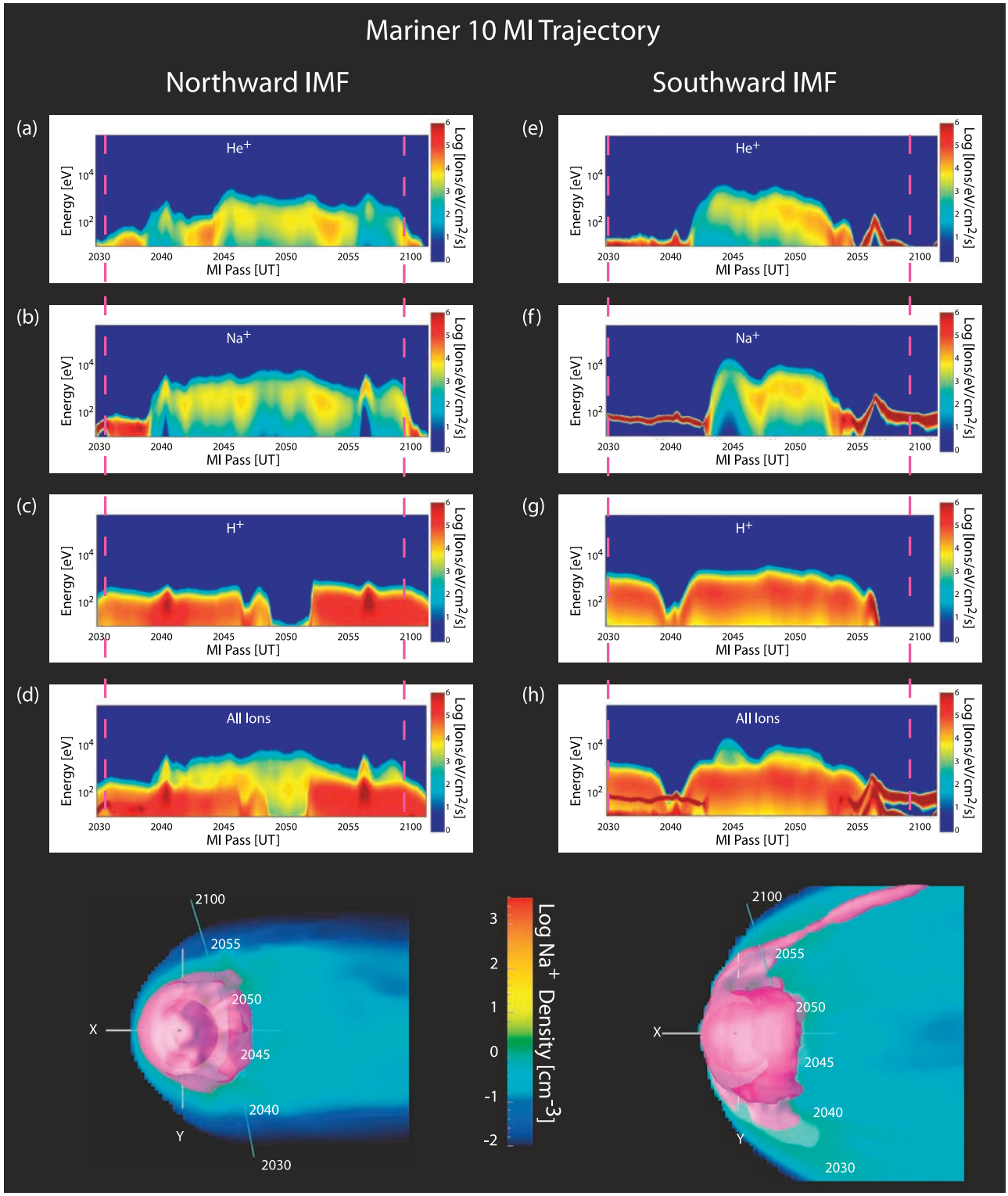

Figure 4. Synthetic spectrograms for the Mercury I trajectory of the Mariner 10 spacecraft on 29 March 1974. Pink dashed lines indicate magnetopause crossings, as determined by the model. Na^+ is accelerated to higher energies than other species under both northward (first column) and southward (second column) IMF conditions.

ions, accelerated along magnetic field lines, will charge exchange with gravitationally bound neutrals [*Lundin et al.*, 1997]. In addition to charge exchange, heavy ions sputter new exospheric neutrals and ions. The transport of sodium ions to higher latitudes may then produce the neutral Na in Figure 3a by either sputtering or charge exchange of Na^+. These ionized neutrals are picked up by the solar wind convection electric field which, given the large gyroradius

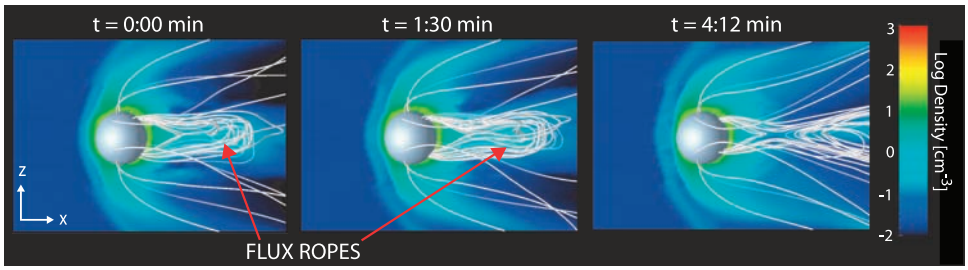

Figure 5. Time evolution of flux rope formation occurring during a fast reconnection event. A flux rope develops in the tail and is ejected a few minutes later as a plasmoid with a core magnetic field of ~20–25 nT. View is of the noon-midnight meridian in all panels and field lines overlaid on the density of the He^+ species.

of Na may, leads to the dawn-dusk asymmetry seen in Figure 2d.

[20] Large variations in heavy ion acceleration seen between times of northward and southward IMF indicate that Na^+ moves toward the polar regions on short times scales and is influenced by magnetospheric effects. Orientation of the IMF in simulations affects the morphology of the open and closed planetary field lines on Mercury, supporting the theory that the magnetosphere's effects are the cause of the north and south neutral Na asymmetries seen by ground-based telescopes [*Potter and Morgan*, 1990].

3.3. Synthetic Spectrograms

[21] Multifluid modeling enables us to generate synthetic spectrograms along any desired trajectory to compare energy and flux measurements with satellite data. By recording the velocity, temperature and density of each ion population along the path for any model trajectory, and assuming a Maxwellian the probability distribution is determined. The Mercury I pass of the Mariner 10 spacecraft is the trajectory used in Figure 4. Figure 4 shows synthetic spectrograms for both northward (first column) and southward (second column) IMF conditions, and includes all three of the ion species over an energy range from 10 eV to 10 keV.

[22] Magnetopause crossings are indicated by pink dashed lines and the trajectory transitions from open to closed magnetic field lines at ~2040 and back shortly after 2055. During northward IMF the Na^+ population (Figure 4b) is accelerated to higher energies than either solar wind protons (Figure 4c) or ionospheric He^+ (Figure 4a), in agreement with the acceleration of Na^+ Figure 2. There is little solar wind access to the exospheric region at midnight for this trajectory. The primary difference between this case and the same trajectory for southward IMF are that the exospheric ions have higher fluxes, but are confined to a narrow band of low energies for the dusk and dawnside sodium enhancements. The magnetopause boundary is outside the beginning of this trajectory and we see an inflated magnetosphere in the dawn-dusk regions, although the magnetopause is compressed at the subsolar point. As is evident in Figure 4h, the same trajectory, but now with southward IMF, passes through two regions of increased sodium density where Na^+ is accelerated to higher energies. The He^+ population is also accelerated, but not to the same extent as Na^+.

[23] *Boardsen and Slavin* [2007] use Mariner 10 magnetometer data to look for Na ion cyclotron waves and finding few question whether there is enough time to thermalize this expected Na^+ population. In calculating the energy spectrograms we use a streaming Maxwellian where the drift speed is much greater than the thermal velocity, so our use of an azimuthally symmetric Na^+ population is reasonable. Although the multifluid model does not include nongyrotropic effects and instabilities, it has been shown to resolve many of the ion-cyclotron effects observed in hybrid codes [e.g., *Harnett et al.*, 2005].

3.4. Flux Rope Generation

[24] An example of how the Hermean tail is altered by orientation of the IMF is shown in Figure 5; fast reconnection occurs with flux ropes developing only a few minutes after the turning of the IMF. The density of Na^+ ions is depleted in a small region of the xy-plane at the same time as a kinking of the current sheet begins to generate flux ropes at this location. This small plasmoid with a core magnetic field evolves and quickly moves downtail over ~4 minutes. This novel prediction of small scale flux ropes in a numerical model is in agreement with *Siscoe et al.*'s [1975] and *Slavin and Holzer*'s [1979] calculations that suggest the flux transfer events seen by Mariner 10 occur on time scales on the order of minutes. An x-line forms at ~2.5 R_M downtail (consistent with *Slavin*'s [2004] prediction), because the planet is small and its field weak, allowing the reconnection line to form closer than at Earth, so that there is rapid penetration of the electric field into the Hermean magnetosphere. Flux ropes are present in both the magnetotail and dayside magnetopause regions. The magnetopause flux ropes (not shown) are on the scale of ~0.1 R_M and those in the tail are ~1 R_M in length. After reconnecting, a plasmoid with an appreciable core magnetic field of ~20–25 nT is ejected downtail. The fast time scales on which flux is transferred in the Hermean magnetosphere supports the conclusion that the solar wind erodes the dayside, enabling the frequent interaction of the solar wind with the planetary surface.

4. Conclusions

[25] Multifluid simulations of Mercury's response to forcing from the solar wind are particularly suited to studies of this system because the heavy Na^+ population within this weak planetary field causes mass effects in the regions of

interest to be all the more striking. This paper confirms the geometry of solar wind proton precipitation for northward and southward IMF and shows that heavy ion outflows are enhanced by nearly an order of magnitude in the presence of an antiparallel magnetic field at the magnetopause. Much of the dayside magnetic field is seen to erode, under conditions more realistic than the extreme solar wind speeds required by MHD models, indicating that erosion of magnetic flux in the dayside under typical solar wind conditions is possible. MHD models do not include mass effects, which enhance the ion loss and mass loading of the solar wind. It is also shown that small-scale flux ropes are present in the magnetotail during reconnection, and that this reconnection occurs on very short time scales and relatively much closer toward the planet than at Earth, as a result of Mercury's small size and weak planetary field.

[26] The minute time scales on which these reconnection events occur agrees with those on which depolarization signatures and several energetic particle injections were seen in the first Mariner 10 pass [*Siscoe et al.*, 1975]. Mercury's small magnetosphere, and size of the planet relative to the large gyroradius of the heavy ions, appear to modulate these dynamic processes and cause reconnection to occur faster than at Earth. The multifluid model is the first global 3-D model to quantify the outflow of sodium ions under different conditions and thus confirm ground-based observations of the dynamic nature of the neutral sodium population. Variation and asymmetry of the outflowing Na^+ plumes is an IMF influenced magnetospheric effect. Future work will examine the role $|B_y|$ plays in the development and movement of the asymmetries seen at the north and south poles by driving the asymmetry with the convection electric field. As Mercury's magnetospheric interaction with the solar wind continues to be probed and predicted in anticipation of the MESSENGER and Bepi-Columbo missions, small-scale processes such as high-latitude sodium enhancements and flux ropes will play an important role in the morphology of the global magnetosphere.

[27] **Acknowledgments.** This work was funded by NSF grant 0617654 and NASA grant NNG05GL9G.

[28] Amitava Bhattacharjee thanks the reviewers for their assistance in evaluating this paper.

References

Boardsen, S. A., and J. A. Slavin (2007), Search for pick-up ion generated Na^+ cyclotron waves at Mercury, *Geophys. Res. Lett.*, *34*, L22106, doi:10.1029/2007GL031504.

Broadfoot, A. L., S. Kumar, M. J. S. Belton, and M. B. McElroy (1974), Mercury's atmosphere from Mariner 10: Preliminary results, *Science*, *185*, 166–169.

Harnett, E. M., and R. M. Winglee (2007), High-resolution multifluid simulations of the plasma environment near the Martian magnetic anomalies, *J. Geophys. Res.*, *112*, A05207, doi:10.1029/2006JA012001.

Harnett, E. M., R. M. Winglee, and P. A. Delamere (2005), Three-dimensional multi-fluid simulations of Pluto's magnetosphere: A comparison to 3D hybrid simulations, *Geophys. Res. Lett.*, *32*, L19104, doi:10.1029/2005GL023178.

Hunten, D. M., D. E. Shemansky, and T. H. Morgan (1988), The Mercury atmosphere, in *Mercury*, edited by F. Vilas, C. R. Chapman, and M. S. Matthews, pp. 562–612, Univ. of Ariz. Press, Tucson.

Ip, W. H., and A. Kopp (2002), MHD simulations of the solar wind interaction with Mercury, *J. Geophys. Res.*, *107*(A11), 1348, doi:10.1029/2001JA009171.

Kabin, K., T. I. Gombosi, D. L. DeZeeuw, and K. G. Powell (2000), Interaction of Mercury with the solar wind, *Icarus*, *143*, 397–406.

Kallio, E., and P. Janhunen (2003a), Modelling the solar wind interaction with Mercury by a quasi-neutral hybrid model, *Ann. Geophys.*, *21*, 2133–2145.

Kallio, E., and P. Janhunen (2003b), Solar wind and magnetospheric ion impact on Mercury's surface, *Geophys. Res. Lett.*, *30*(17), 1877, doi:10.1029/2003GL017842.

Killen, R. M., and W. H. Ip (1999), The surface-bounded atmospheres of Mercury and the Moon, *Rev. Geophys.*, *37*, 361–406.

Krall, N. A., and A. W. Trivelpiece (1973), *Principles of Plasma Physics*, p. 95, McGraw-Hill, New York.

Luhmann, J. G., C. T. Russell, and N. A. Tsyganeko (1998), Disturbances in Mercury's magnetosphere: Are the Mariner 10 "substorms" simply driven?, *J. Geophys. Res.*, *103*, 9113–9119.

Lundin, R., S. Barabash, P. Brandt, L. Eliasson, C. M. C. Nairn, O. Norberg, and I. Sandahl (1997), Ion acceleration processes in the Hermean and terrestrial magnetospheres, *Adv. Space Res.*, *19*(10), 1593–1607.

McClintock, W. E., and M. R. Lankton (2007), The Mercury Atmospheric and Surface Composition Spectrometer for the MESSENGER Mission, *Space Sci. Rev.*, *131*, 481–522, doi:10.1007/s11214-007-9264-5.

Ness, N. F., K. W. Behannon, R. P. Lepping, and Y. C. Whang (1975), Magnetic field of Mercury confirmed, *Nature*, *255*, 204–205.

Paty, C., and R. Winglee (2006), The role of ion cyclotron motion at Ganymede: Magnetic field morphology and magnetospheric dynamics, *Geophys. Res. Lett.*, *33*, L10106, doi:10.1029/2005GL025273.

Potter, A. E., and T. H. Morgan (1985), Discovery of sodium in the atmosphere of Mercury, *Science*, *229*, 651–653.

Potter, A. E., and T. H. Morgan (1986), Potassium in the atmosphere of Mercury, *Icarus*, *67*, 336–340.

Potter, A. E., and T. H. Morgan (1990), Evidence for magnetospheric effect on the sodium atmosphere of Mercury, *Science*, *248*, 835–838.

Potter, A. E., R. M. Killen, and T. H. Morgan (1999), Rapid changes in the atmosphere of Mercury, *Planet. Space Sci.*, *37*, 1441–1448.

Potter, A. E., R. M. Killen, and T. H. Morgan (2002), The sodium tail of Mercury, *Meteorit. Planet. Sci.*, *37*, 1165–1172.

Russell, C. T., D. N. Baker, and J. A. Slavin (1988), The magnetosphere of Mercury, in *Mercury*, edited by F. Vilas, C. R. Chapman, and M. S. Matthews, pp. 514–561, Univ. of Ariz. Press, Tucson.

Siscoe, G. L., N. F. Ness, and C. M. Yates (1975), Substorms on Mercury?, *J. Geophys. Res.*, *80*, 4359–4363.

Solomon, S. C., et al. (2001), The MESSENGER mission to Mercury: Scientific objectives and implementation, *Space Sci. Rev.*, *49*, 1445–1465.

Slavin, J. A. (2004), Mercury's magnetosphere, *Adv. Space Res.*, *33*(11), 1859–1874.

Slavin, J. A., and R. E. Holzer (1979), The effect of erosion on the solar wind stand-off distance at Mercury, *J. Geophys. Res.*, *84*, 2076–2082.

Winglee, R. M. (2004), Ion cyclotron and heavy ion effects on reconnection in a global magnetotail, *J. Geophys. Res.*, *109*, A09206, doi:10.1029/2004JA010385.

E. M. Harnett, A. Kidder, and R. M. Winglee, Department of Earth and Space Sciences, University of Washington, Box 351310, Seattle, WA 98195, USA. (ariah@ess.washington.edu)